Quantitative analysis of plasmon excitations in hard x-ray photoelectron spectra of bulk black phosphorus

Denis G.F. David, Christian Godet, Fredrik O.L. Johansson, Andreas Lindblad

Quantitative analysis of plasmon excitations in hard x-ray photoelectron spectra of bulk black phosphorus

Denis G.F. David[a], Christian Godet[b,*,Christian.godet@univ-rennes1.fr], Fredrik O.L. Johansson[c], Andreas Lindblad[c,*,andreas.lindblad@physics.uu.se]

[a]Instituto de Física, Universidade Federal da Bahia, Campus Universitário de Ondina, 40.210-340 Salvador, Bahia, Brazil

[b]Univ Rennes1, CNRS, IPR (Institut de Physique de Rennes) - UMR 6251, F-35042 Rennes, France

[c]Div. Inorganic Chemistry / Dept. Chemistry (Ångström), Uppsala University, SE-752 21 Uppsala, Sweden
[*]Corresponding authors.

Graphic abstract

Highlights

- Energy loss distribution of P 1s photoelectrons in black phosphorus
- Discrimination of plasmon excitations and inter band transitions
- Anomalous surface plasmon resonance at 9 eV
- DFT calculated ELF tensor vs measured ELF

Abstract

Black phosphorus (BPh) is a layered material with strong in-plane anisotropy of its structural and electronic properties; in spite of the great potential of BPh for conceptually new devices in optoelectronics and plasmonics, its fundamental electronic excitations have not yet been fully elucidated. In order to discriminate collective (plasmons) and single-particle (inter band transitions) excitations, we investigate the energy-loss distribution of P 1s photoelectrons in hard X-ray photoelectron spectra of BPh over a wide energy range. The energy-loss function (ELF), averaged over the principal directions of the BPh crystal, has been retrieved by using a Fourier Transform analysis to eliminate multiple inelastic scattering events. At low loss energies (1-8 eV), weak unresolved energy loss peaks are well described by DFT calculated inter band transitions, showing some anisotropy in the dielectric function $\varepsilon(\omega, q)$ tensor of BPh. At high loss energies, the ELF is dominated by the collective excitation of valence electrons with a peak energy at 20.1±0.2 eV, weak anisotropy is found in the DFT calculated Im$(-1/\varepsilon)$ tensor. The anomalously small peak energy (9.0±0.5 eV) of a weak surface plasmon resonance is attributed either to low surface electron density in the terminal phosphorene layer or to some anisotropic surface plasmon propagation.

Keywords: black phosphorus, XPS, HAXPES, energy loss, plasmon

1. Introduction

Black Phosphorus (BPh) is the thermodynamically stable phosphorus allotrope, with a puckered orthorhombic structure (***a*** = 0.331 nm, ***b*** = 1.048 nm, ***c*** = 0.438 nm, $\alpha = \beta = \gamma = 90°$) and high atom density ($N_{AT} = 5.23\times10^{28}$ m^{-3}, $\rho = 2690$ kg.m^{-3}) **[1-5]**. BPh is formed by a stack of two-dimensional (2D) phosphorene layers held together by weak van der Waals forces. Within the phosphorene layer, each sp^3-hybridized P atom is covalently bonded to three neighbors, with two bonds within the same plane, and a third bond connecting P atom located at the top and bottom of the phosphorene layer (**Fig. 1**). Hence, in contrast with graphene where the carbon monolayer is strictly flat, BPh has a puckered structure, where each single sheet can be seen as a bilayer of P atoms.

Intensive search for tunable 2D materials beyond graphene for electronic and opto-electronic applications **[5-9]** has boosted scientific interest in BPh as a semiconductor with a narrow (0.31-0.35 eV) direct band gap and high carrier mobility **[10-13]**. The in-plane structural anisotropy (**Fig. 1**), with armchair configuration in the *x*-direction (***c*** axis) and zig-zag configuration in the *y*-direction (***a*** axis) **[1]**, results in strong anisotropy of the dielectric function $\varepsilon(\omega, q)$ **[14]**, electron and hole effective masses **[15]** or phonon properties **[8]** within the *x*-*y* plane.

Such unique electronic, optical, transport, thermal and mechanical properties can be exploited in the design of conceptually new devices, e.g. field effect transistors **[7, 8, 16, 17]**, optoelectronic devices **[17, 18]** and plasmonic applications **[8, 19, 20].** Besides the above applications, BP has also been tested as a new material for water splitting, photovoltaic solar cells and photodetectors **[5, 6, 17, 21]**. For sensors and electrochemical energy-storage devices **[21]**, BPh possesses a much higher surface to volume ratio than most other available 2D layered materials because of its puckered lattice configuration.

Different approaches have been used for band structure calculations, including tight binding **[22-24]** or self-consistent pseudopotential **[24]** methods, and density functional theory (DFT) **[25-30]**. Theoretical calculation of the orbital-resolved DOS shows that the upper valence band is dominated by p_z orbitals while deeper states have mostly p_x and p_y character. The electronic structure of BPh has been experimentally investigated using photoelectron spectroscopies. The valence band density of states (DOS) has been characterized by X-ray Photoelectron Spectroscopy (XPS) **[14, 31-33]** and by angle-resolved UPS **[30, 34, 35]**. In addition, photoelectron diffraction reveals that the structure of the top phosphorene layer is very similar to that expected for the bulk, indicating weak interaction between the bilayers **[4]**. Surface studies require a controlled cleavage because UV-assisted oxidation occurs upon exposure of BPh to air and water **[36-39]**.

In XPS spectra, for both P 2s and P 2p core levels, well-defined photoelectron energy loss peaks (observed up to second order) were attributed to plasmon excitations; the bulk plasmon energy E_{BP} ≈ 20.0±0.2 eV **[14, 31-33]** found in photoelectron energy loss spectroscopy (PEELS) is slightly higher than the loss energy in EELS spectra (19.3 eV) **[36]**. This collective and coherent oscillation at E_{BP} ≈ 20.0±0.2 eV involves all valence band electrons (five per P atom). However, the bulk plasmon in BPh shows a single main peak, in contrast with many 2D layered materials, such as graphite [**40-41**], transition metal dichalcogenides (TMD) [**42-43**] and boron nitride *h*-BN [**44-45**], where a subset of occupied valence band states is involved in some additional low-energy plasmon; this so-called π plasmon (as opposed to the high energy $\sigma+\pi$ plasmon which involves all valence band electrons) observed for in-plane momentum transfer is generally found below 10 eV.

Although BPh offers a great potential for conceptually new devices in optoelectronics and plasmonics, its fundamental electronic excitations have not yet been fully elucidated. In this work, in order to discriminate collective and single-particle excitations, we investigate the loss energy distribution of P 1s photoelectrons in hard X-ray photoelectron spectra (HAXPES) of BPh over a wide energy range. Two consequences arise from the large photoelectron kinetic energy value (E_0): a) HAXPES is essentially a bulk technique related to the relatively small inelastic scattering rate, i.e. large inelastic mean free path (IMFP); b) in the low loss-energy range, the observation of weak inter band transitions (IBT) is favoured due to a strong decrease of the probability of exciting surface plasmon modes [**46**].

Section 2 describes experimental details and DFT calculations of the electronic structure. HAXPES has been used for the first time to measure the energy-loss distribution of P 1s photoelectrons (binding energy 2144.0 eV) with a monochromatic synchrotron source. In anisotropic crystals, DFT calculation of the orbital-resolved density-of-states (DOS) distributions, dielectric function tensor < $\varepsilon(\omega, q)$ > and loss function tensor < Im($-1/\varepsilon(\omega, q)$) > is crucial for the interpretation of the effective energy loss function (ELF), e.g. to discriminate collective vs single-particle energy loss mechanisms.

Section 3 details the procedure for a quantitative analysis of HAXPES-PEELS data. Well-defined equidistant energy-loss peaks correspond to successive plasmon excitations. Their spectral distribution being described by multiple convolution products of the ELF distribution corresponding to a single excitation, the Fourier Transform (FT) method described previously [**47**] is well suited to analyze PEELS data in order to retrieve the energy loss function. This classical dielectric model assumes identical ELF distributions for intrinsic plasmon production (sudden creation of a core

hole) and extrinsic plasmon excitation along the electron path across the solid to the surface. Note that, in contrast with metals [**48, 49**], the shape of the core level peaks in the BPh semi-conductor is quasi-symmetrical; hence a small overlap is found between the zero-loss peak (ZLP) tail and the surface plasmon (SP) or bulk plasmon (BP) distributions.

In **Section 4**, the retrieved ELF is compared with the dielectric function and energy loss function derived from the DFT calculated electronic structure, along the BPh crystal principal axes. The ELF is dominated by a bulk plasmon at 20.1 eV while a weak energy loss peak near 9 eV is attributed to some surface plasmon resonance, since no significant inter band transition occurs in the latter energy range. Weak unresolved loss peaks at low energy (1-8 eV) are attributed to inter band transitions.

The retrieved ELF represents a weighted average over the principal directions of the BPh crystal. In our HAXPES experimental conditions, at normal emission angle, the **Appendix** shows that the typical orientation of the plasmon wave vector, with respect to the principal crystal axes, provides efficient averaging of the anisotropic dielectric properties of BPh over the principal axes.

2. Experiment and spectral analysis

2.1 HAXPES experiment

Hard X-ray Photoelectron Spectroscopy (HAXPES) experiments were performed at the Bessy II synchrotron radiation facility (Helmholtz-Zentrum Berlin) at the double crystal monochromator equipped dipole beamline KMC-1 **[50]** and the high kinetic energy (HIKE) end-station [**51**]. For the overview XPS spectra obtained at 3 keV X-ray energy, the first order harmonic of a Si(111) crystal was used. The P 1s core-level spectrum was recorded using the third harmonic of 2005 eV, *i.e.* 6015 eV X-ray energy. The large value of the photoelectron inelastic mean free path in BPh, $\lambda(E_0 = 3870$ eV) ≈ 7.7 nm, derived from the TPP-2M model [**52**] (using the atom density, $N_{AT} = 5.23\times10^{28}$ m^{-3}, the plasmon energy, $E_P = 20$ eV, and the average IBT energy, $E_{IB} \approx 5$ eV) confirms the fact that HAXPES is a bulk technique.

The X-ray beam, oriented at grazing incidence, was linearly polarized with the polarization vector pointing out of the *x*-*y* plane (*z* direction). In this geometry, the differential photoelectric cross-section is maximized at normal emission angle **[53]** (**Appendix A**). Electrons ejected from the sample near normal emission were collected using a VG Scienta R4000 electron analyzer with pass energy of 100 eV in transmission mode with ±16° acceptance angle. The P 1s line shape results from a convolution between the Lorentzian distribution of the core level excitation which

corresponds to the lifetime, and the Gaussian instrumental broadening which combines beamline and spectrometer broadening functions; in our experimental conditions (**Fig. 2**), the P 1s Lorentzian width (FWHM = 0.42 eV) is larger than the Gaussian broadening (FWHM = 0.32 eV), hence the latter weakly affects the measured HAXPES spectra of BPh.

A commercial (HQgraphene **[54]**) high purity (> 99.995 %) black phosphorus single crystal was prepared by cleaving the crystal in UHV using a roll of Kapton tape. XPS overview spectra (**Fig. 2**, inset) were measured with better surface sensitivity (smaller IMFP) using lower X-ray energy (3100 eV); the binding energies (BE) were measured for the core level peaks P $2p_{3/2}$ at 129.87 eV, P $2p_{1/2}$ at 130.72 eV and P 2s at 187.72 eV. Small carbon (0.7 at.%) and oxygen (3.9 at.%) adventitious contamination is probably due to adsorption of residual gases (base pressure in the 10^{-9} mbar range) since no indication of phosphorus oxide appears in the measured valence band or survey spectra (BE expected near 2150 eV (P 1s) or 135.8 eV (P 2p) for phosphorus pentoxide P_4O_{10} **[55]**).

2.2 Physics of plasmon excitation

XPS-PEELS data analysis in isotropic materials has been described in detail elsewhere **[37]**. Photoelectron inelastic scattering excites a plasmon with energy E_P and wave vector q; energy and momentum conservation rules provide the plasmon wave vector q-components parallel ($q_{\parallel}$) and perpendicular ($q_{\perp}$) to the initial electron trajectory **(Appendix A)**. For each value of the loss energy T distribution, the sensitivity given by the Bethe-Born factor $f_C(T)$ is obtained by integration over all scattering angles, ϑ, up to a cutoff value ϑ_C (or cutoff wave vector q_C) above which plasmons decay into electron-hole pairs (Landau damping) **[56]**. For P 1s photoelectrons with E_0 = 3870 eV, the physically allowed range for plasmon wave vector values is between q^- = 0.84 nm^{-1} (ϑ = 0) and q_C = 12.7 nm^{-1} (ϑ_C = 40 mrad = 2.3°) at the main loss peak energy $T = E_P$ = 20 eV.

In contrast with laboratory XPS equipment producing core level photoelectrons with moderate kinetic energy (E_0 < 1.5 keV in most cases), large photoelectron kinetic energy up to 12 keV may be obtained from synchrotron radiation in HAXPES experiments. Larger E_0 values result in smaller inelastic scattering rate, i.e. larger inelastic mean free path, and some attenuation of the surface excitation parameter (SEP) which represents the average number of surface plasmon excitation events per emitted photoelectron crossing the surface [**46**].

In anisotropic solids, the orientation of the plasmon wave vector q with respect to the principal crystal axes depends on scattering angle and energy loss values (**Appendix A**). Due to the kinematic factor $\theta/\left(\vartheta^2 + \vartheta_T^2\right)$ where $\theta_T = T/2E_0$, **[57-59]**, the inelastic scattering probability is dominated by a narrow range of small scattering angles, close to ϑ_T (ϑ_T = 2.6 mrad = 0.15° at ELF

peak energy $T = E_P = 20$ eV in BPh). This dominant angular range is depicted in **Fig. A1** by the bold vertical lines for some relevant energy values in the ELF distribution. The corresponding angle β with respect to the z normal-axis is expected in the range $35° < \beta < 55°$. This result obtained for HAXPES experimental conditions shows that plasmon excitation mechanisms provide efficient averaging of the in-plane and out-of-plane dielectric properties. This situation is typical of high kinetic energy values, E_0, in contrast with laboratory XPS experiments which are experimentally more sensitive to the out-of-plane loss function.

2.3 Fourier Transform analysis of PEELS data

No arbitrary background removal is performed in the PEELS distribution since all energy losses are assigned to plasmon excitations along with some inter band transitions, in line with previous assumptions [**47, 57, 60, 61**]. In this work, intrinsic plasmon excitations are overlooked [**47**] and the ELF is supposed to be independent of the photoelectron creation depth.

In order to eliminate multiple-order losses, the FT algorithm requires accurate determination of zero-loss peak (ZLP) line shape, energy distribution of the X-ray photon source and electron analyzer resolution **[47]**. The ZLP is modeled as a convolution between Gaussian experimental broadening (FWHM = 0.31 eV, σ = 0.187 eV) and Lorentzian natural line shape of the P 1s core level in BPh (FWHM = 2Γ = 0.426 eV). For metals, PEELS data analysis must take into account the ZLP asymmetry due to low energy excitations between valence and conduction band states [**48-49**]; in contrast, the very small ZLP asymmetry factor, $\alpha < 0.01$, found in BPh is typical of semiconducting materials.

2.4 DFT calculation

Knowledge of the electronic structure is important to discriminate collective vs single-electron loss mechanisms. In the case of BPh, the loss peak at 20 eV is clearly due to plasmon excitations; however, more information about inter band transitions is needed to understand the origin of the weaker loss peak near 9 eV.

The electronic ground state of BPh was calculated with the density functional theory (ABINIT code) in the Perdew–Burke–Ernzerhof generalized gradient approximation (DFT-GGA) of the exchange-correlation functional, using norm-conserving Goedecker pseudo-potentials (HCTH-120) [**62-64**]. Experimental lattice parameters taken from the Library of Crystallographic Prototypes [**3, 65**] are in excellent agreement with **Ref. 14**, after referential axes permutation: (x, y, z) → (y, z, x).

In order to get the dielectric function for the three principal axes of the crystal, a computation of the ground state involving the first 10 bands plus 40 empty bands was made, followed by a computation of the real and imaginary parts of the dielectric function with the Optic module. The Brillouin zone was sampled using a 16 × 16 × 16 Monkhorst-Pack mesh of special *k* points **[66].** The gap of BPh found at 0.1 eV was increased to the experimental value of 0.35 eV by a scissors operation. Partial joint density-of-states, JDOS $[l = i \rightarrow l = j]$, were also calculated from angular momentum resolved partial density-of-states distributions. Anisotropic dielectric functions and energy loss functions of BPh were finally obtained for the principal directions of the crystal.

3. Results

The bulk energy-loss function (averaged over the principal directions of the BPh crystal) is derived from HAXPES-PEELS data analysis and compared with the anisotropic electronic structure of BPh obtained from DFT calculations in order to discriminate collective vs single-particle loss mechanisms. The main loss peak is clearly a strong bulk plasmon at energy $E_{BP1} \approx 20$ eV. However, particular attention is given to the broad loss peak observed near 9 eV; this loss mechanism cannot be mistaken with the corresponding surface plasmon expected near $E_{SP1} \approx 14$ eV for an abrupt surface. As discussed in **Section 4,** it is attributed to a collective excitation mechanism since no significant inter band transition is expected at this particular energy.

3.1 HAXPES-PEELS data analysis

Figure 2 shows the photoelectron current emitted from the black phosphorus crystal near normal emission angle, as a function of binding energy (BE). The P 1s core level peak is found at 2144.04±0.05 eV (using Au 4f $_{7/2}$ BE of 84.0 eV), in excellent agreement with previous studies **[55]**. A series of equidistant replicas is observed on the low kinetic energy side of this zero-loss peak (ZLP, kinetic energy $E_0 \approx 3870$ eV). HAXPES shows multiple bulk plasmon excitations up to sixth order, over a very wide energy range without overlap with any other core level peak (surface contaminants only occur at small BE, see inset of **Fig. 2**).

Energy loss spectra have been normalized at zero-loss peak energy (taken at P 1s peak maximum) after removal of a flat background (1.02×10^4 CPS in **Fig. 2**) taken from the high kinetic energy side of the ZLP. After subtraction of a symmetrical ZLP (**Fig. 3**), extrapolation of the low energy loss distribution gives a small finite gap value, E_G = 0.3±0.1 eV; however, the remaining loss signal below 1 eV (not shown) is very sensitive to the precise adjustment of the ZLP position. The main asymmetric loss peak (E_{BP1}) is identified as a bulk plasmon; the corresponding surface plasmon excitation expected at energy $E_{SP1} \approx E_{BP}/\sqrt{2}$, for an abrupt surface, is merged with the broad bulk

loss distribution. The loss feature near 9 eV will be attributed to a surface collective excitation (E_{SP2}), as discussed in **Section 4**. Besides these collective excitation modes, single-electron transitions are expected in the low energy region, mainly below 10 eV, as shown in **Section 3.2**.

Broad photoelectron energy loss features may be expected for several reasons: a) anisotropy in the loss function, b) dispersion of the plasmon energy as a function of the q wave vector magnitude ($q < q_C$), c) self-convolution of the ELF resulting from successive inelastic scattering events. In a first step, the latter broadening effect is eliminated using the FT method described in **Section 2.3**. The FT algorithm includes a tunable noise filtering stage to obtain the energy loss function (**Fig. 4a**, black curve**)**; the inset shows that multiple order losses have been properly suppressed over the whole spectrum up to 120 eV. Removal of second order losses results in narrower plasmon peak at 20 eV along with better resolved energy loss peaks near 9 and 5.5 eV.

In a second step, analytic decomposition of the ELF of BPh, retrieved using the FT method, has been performed within a simple dielectric theory of plasmon excitation. Drude-Lorentz loss functions for bulk (E_{BP1}) and surface (E_{SP1}) excitations were adjusted to the ELF in the range 12-26 eV. Fast convergence is obtained for the BP peak parameters: $E_{B1} \approx 20.1\pm0.2$ eV, $\Gamma_1 \approx 5.1\pm0.2$ eV. Although the surface plasmon intensity remains rather arbitrary at normal emission angle, in the absence of angular HAXPES data, the surface excitation probability ($\mathrm{SEP}_1 = A_{\mathrm{SP1}}/(A_{\mathrm{SP1}} + A_{\mathrm{ZLP}}) \approx 0.07\pm0.02$) derived from the area of the positive part of SP1 (A_{SP1}) relative to the ZLP area (A_{ZLP}) in **Fig. 4b** is consistent with Pauly's model [**46**].

The weaker collective excitation is described by a second Drude-Lorentz loss function, with $E_2 \approx 10.0\pm0.3$ eV, $\Gamma_2 \approx 6.5\pm1$ eV. Both position and width are constrained by the observed peak near 9 eV and the intensity is chosen to obtain a monotonic decrease of the residual loss in the range 3-13 eV (black curve in **Fig. 4b**). The residual signal above 13 eV (small peaks at 16 and 20 eV) shows some deviation of the BP1 line shape from a single Drude-Lorentz ELF.

After removal of the collective excitations in the ELF distribution, the residual energy losses show a broad structure made of several unresolved peaks below 10 eV (**Fig. 4b**) which represent weak contributions with respect to the collective excitations. The energy loss mechanisms in this energy region are attributed to inter band transitions between occupied VB states and unoccupied CB states. Although a decomposition is beyond the scope of this work, some interpretation is discussed in **Section 4** using the orbital-resolved density of electronic states (**Fig. 5a**) and the dominant transition matrix elements for *s* and *p* orbitals (**Fig. 5b**), derived from DFT calculations.

3.2 Electronic structure of the anisotropic BPh crystal

The DOS distribution in the valence and conduction bands and the dielectric function tensor of BPh obtained from ABINIT calculations are very similar to previous reports **[1, 14]**. The electronic structure characteristics along the principal axes: Re(ε), Im(ε), Im(-1/ε), are reported in figures **6a**, **6b** and **6c** respectively.

In the calculated loss functions, Im($-1/\varepsilon$), strong anisotropy is found at low energies, typically below 4 eV, and weak anisotropy in the range 4-8 eV (not shown). The main loss peak is a bulk plasmon resonance located at very similar energy ($E_{BP1} \approx$ 19.8±0.2 eV) along the principal axes (**Fig. 6c**). However, detailed examination shows that the BP1 peak is located at slightly higher energy for the armchair direction, while its width is larger for the zig-zag direction and smaller for the arm-chair direction. The BP1 plasmon peak asymmetry (skewed exponential on the low energy side) is found for all q directions. Interestingly, in the zig-zag direction, oscillatory behavior near the peak maximum and some loss feature near 15.5 eV may correspond to the deviation of PEELS experimental loss from a single Drude-Lorentz function, as observed in **Fig. 4b**.

The dielectric function of BPh calculated along the principal crystal axes shows a wide distribution of unresolved absorption peaks, the most prominent ones being located between 3.5 and 6 eV (**Fig. 6b**). As a matter of fact, in $\varepsilon_2(E)$ spectra, calculated inter band transitions in BPh appear to be quite weak above 7 eV. Our DFT results indicate a weak feature at about 8 eV in the armchair (out-of-plane) orientation, similar to previous results **[14]**; in contrast, first principles calculations **[28]** show no IBTs in $\varepsilon_2(E)$ spectra for both in-plane orientations, in the range 6-10 eV. In conclusion, since no IBT peak can be detected at 9 eV in Im(ε) for all principal axes, the observed weak loss feature at 9 eV must have a collective excitation origin.

4. Discussion

Peaks in the energy loss function may be associated either with a plasmonic collective oscillation of valence electrons **(Section 4.2)** or with inter band transitions **(Section 4.1)**. The former generally dominates among the inelastic scattering mechanisms. Collective and single electron phenomena can be discriminated if the dielectric function in the vicinity of such peaks is known, i.e. there is a peak in ε_2 due to some inter band transition when ε_1 crosses zero with a negative slope, whereas the collective excitation with plasmon peak in the loss function Im($-1/\varepsilon$) occurs when ε_1 crosses zero with a positive slope **[40, 67]**. In the latter case, if ε_2 is not a small quantity, a plasma-like resonance condition is given by:

$$(\varepsilon_1{}^2 - \varepsilon_2{}^2)\frac{d\varepsilon_2}{d\omega} - 2\varepsilon_1\varepsilon_2\frac{d\varepsilon_1}{d\omega} = 0$$

characterized by a broad and weak loss peak in Im($-1/\varepsilon$). The width of this plasma-like resonance is approximately given by the inverse slope $(d\varepsilon_1/d\omega)^{-1}$. Note that the condition $\varepsilon_1 = 0$ is retrieved for small ε_2 values and such singularity corresponds to charges that oscillate coherently and collectively. Additional complexity is expected in anisotropic crystals, hence calculations of the band structure and optical properties are very useful in order to establish the collective character of the loss peaks or to assign the main IBTs to particular components of the ε tensor.

4.1 Interband transitions

The small electronic gap (0.3±0.1 eV) estimated from the experimental ELF data confirms the semiconducting character of BPh. The weak unresolved loss peaks observed in the raw HAXPES spectrum at low energy (1-8 eV) are well above the phonon excitation range **[68]**. Since bulk and surface plasmon excitations usually provide broad (several eV wide) spectral features, the rather sharp loss features observed in **Fig. 3**, particularly just above the onset of the energy loss spectrum, are tentatively attributed to inter band transitions between bonding 3s / 3p and antibonding 3s* / 3p* orbitals.

This hypothesis is confirmed by the spectral weight of inter band transitions (after subtraction of plasmon losses) with main peaks located at 2.6 eV, 3.4 eV and 5.1 eV (**Fig. 4b**). HAXPES data at low loss energy are qualitatively described by the sum of partial joint-density of states JDOS[$l = 1 \rightarrow l = 1$] + JDOS[$l = 1 \rightarrow l = 0$] + JDOS[$l = 0 \rightarrow l = 1$], divided by the squared energy value (**Fig. 5b**). Interestingly, good agreement with band structure calculations is obtained without any fitting parameter or selection rules.

Using now the total JDOS, i.e. for transitions including all q values, as an approximation of the imaginary dielectric function, $Im(\varepsilon)$, the corresponding real part $Re(\varepsilon)$ has been derived from its KK transform; the resulting loss function is very close to the BP1 loss distribution, both in peak energy and peak width (not shown). Consistency between the inter band transition distribution and the main plasmon excitation has finally been checked, and a satisfactory Bethe sum rule has been obtained for the number of electrons per atom (N_{EFF} = 4.8) involved in the BP resonance.

Some tentative identification of the observed inter band transitions at 2.6 eV, 3.4 eV, 5.1 eV, 8.0 eV in **Fig. 4b**, to their parent peaks in the respective anisotropic dielectric function indicates that all polarizations contribute to the losses:

● the IBT at 2.6 eV is consistent with in plane armchair ε_2 (q // $\boldsymbol{c}$) contribution.

● the IBT observed at 3.4 eV is attributed essentially to in-plane zig-zag $\varepsilon_2(q \,//\, \boldsymbol{a})$ contribution.

● the IBT found at 5.1 eV is well-matched by the calculated out-of-plane ε_2 ($q \,//\, \boldsymbol{b}$) response, and possibly to the in-plane zig-zag $\varepsilon_2(q \,//\, \boldsymbol{a})$ contribution.

● the very weak IBT detected at 8.0 eV is consistent with some in plane armchair ε_2 ($q \,//\, \boldsymbol{c}$) contribution.

In conclusion, this analysis shows the capabilities of HAXPES-PEELS studies for extracting spectroscopic information about multiple unresolved inter band transitions at low loss energies (1-10 eV), after careful subtraction of the much stronger collective excitation modes.

4.2 Plasmon excitations

The energy loss of P 1s photoelectrons at energy $E_{\mathrm{B1}} \approx 20.1 \pm 0.2$ eV is unambiguously identified as a bulk plasmon excitation, in good agreement with previous analysis of P 2s and P 2p core levels of BPh **[14, 31-33]**. Its position is consistent with the free electron gas value expected at $E_{\mathrm{P\,FE}} = 19.0$ eV (**Appendix A**), which may be shifted upward by the inter band transitions according to $(E_{\mathrm{B1}})^2 = (E_{\mathrm{P\,FE}})^2 + (E_{\mathrm{IB}})^2$, where E_{IB} is the average inter band transition energy. The BP1 peak width ($\Gamma_1 \approx 5.1 \pm 0.2$ eV) is attributed to plasmon dispersion effects rather than electronic structure anisotropy; in EELS experiments, larger dispersion is found for the zig-zag direction as compared with the armchair direction [**69-70**].

The photoelectron inelastic mean free path between successive bulk plasmon excitations has been derived from this HAXPES-PEELS analysis. The IMFP, $\lambda(E_0 = 3870$ eV) $\approx 6.8 \pm 0.5$ nm, in BPh is slightly smaller than the value, $\lambda(E_0 = 3870$ eV) ≈ 7.7 nm, derived from the TPP-2M model [**52**]; this discrepancy may be attributed to the large uncertainty in the β value (i.e. slope of $\left(E/\lambda E_P^2\right)$ $vs\ Ln(\gamma E)$) which is a difference between small parameter values in the TPP model. In addition, the TPP-2M formulae were established essentially for $E_0 < 2$ keV.

As far as the small loss peak near 9 eV is concerned, it must be assigned to a collective excitation since no inter band transition peak appears at this energy in the calculated Im(ε). In this range, Re $\varepsilon \approx -4$ and depends weakly on energy in the range 7-10 eV (dashed horizontal line in **Fig. 6a**) excepted for the zig-zag orientation; since Re ε does not cross the zero value, bulk collective excitations can be excluded. Surface collective modes are thus considered in the following. In contrast with the energy value, $E_{\mathrm{S}} = E_{\mathrm{B}}/\sqrt{2} = 14.2$ eV, expected for an abrupt surface, the resonance energy has an anomalously small value. Several tentative explanations may be suggested:

a) interplay between surface plasmon and inter band transitions **[33]**: this hypothesis is not confirmed by the above DFT calculations
b) smooth drop of the electron density from its bulk value to zero **[71]**: multipole modes are found at larger loss energy than that of normal (monopole) surface plasmons
c) low surface electron density in the terminal monolayer of 2D quantum wells **[72]**
d) anisotropic surface plasmon propagation in BPh **[69-70]** inducing a peculiar field distribution induced by the oscillating surface charges **[73]**.

Additional geometrical effects due to reconstruction have not been considered yet, such as the buckling among the surface atoms and contraction (-5%) of the puckered terminal layer, along with increased separation from bulk layers, as observed in photoelectron diffraction experiments **[4]**.

4.3 Plasmons in 2D layered materials

A valuable comparison can be made with other layered materials. In prototypical 2D materials, e.g. graphite or transition-metal dichalcogenides ($NbSe_2$, MoS_2) **[42, 74, 75]**, calculated and experimental ELF consist of two prominent resonance features for in-plane-polarization that lie (i) below 10 eV and (ii) above 10 eV, while the former is absent in the out-of-plane polarization spectra. BPh properties are qualitatively similar to other layered materials where a low energy plasmon corresponds to the in-plane dielectric function in a region with large dielectric function anisotropy, whereas the dominant plasmon peak is located in a high energy region with small anisotropy.

In graphite and in some TMD, both loss peaks have been clearly attributed to π plasmon and $\pi+\sigma$ bulk plasmon resonances, while in other layered compounds (e.g. in $NbSe_2$), it has been argued that both plasmons have $\pi+\sigma$ character **[74]**. In black phosphorus, a very weak (a few per cent of BP1 intensity) bulk plasmon near 9 eV is obtained in DFT calculations, only along the zig-zag in plane direction, hence the observed loss peak at 9 eV in HAXPES is tentatively attributed to a surface collective resonance.

5. Conclusion

The electronic properties of BPh have been investigated using the photoelectron energy-loss distribution measured in HAXPES. In our experimental conditions, the distribution of momentum transferred to plasmon excitations provides an efficient averaging of the anisotropic ELF of BPh and additional randomization is expected from elastic scattering and multiple inelastic scattering. Using photoelectrons with kinetic energy favours the observation of weak inter band transitions

(IBT) in the low loss-energy range, due to a decreased probability of exciting surface plasmon modes. The experimental ELF was compared with DFT calculated dielectric function and ELF tensors to discriminate collective vs single-particle loss mechanisms.

At higher loss energies, the ELF is dominated by a collective excitation of valence electrons at E_{BP1} ≈ 20.1 eV; the large width of this bulk plasmon is attributed to dispersion effects (as a function of the wave vector $q < q_C$) since weak anisotropy is found in the DFT calculated Im($-1/\varepsilon$) tensor. The anomalously small energy value, $E_2 \approx 9$ eV, of a weak surface plasmon resonance may arise from low surface electron density in the terminal phosphorene layer or anisotropic surface plasmon propagation in BPh; elucidation of the origin of this surface mode requires additional angular photoemission experiments.

Subtraction of the spectral components related to collective excitations gives access to multiple unresolved inter band transitions, at lower loss energies (1-8 eV), which are well described by DFT calculated inter band transitions; the latter results show some anisotropy in the dielectric function $\varepsilon(\omega, q)$ tensor of BPh and all polarizations contribute to the IBT losses. Consistency between the inter band transition distribution and the main plasmon excitation has been checked, leading to satisfactory Bethe sum rules.

In conclusion, this study shows that HAXPES-PEELS combined with DFT calculations is a powerful tool for the investigation of electronic properties of crystalline solids. Some improvements in the method would require a quantum modeling of intrinsic and extrinsic plasmon excitations, including both volume and surface excitations, with a proper description of the dispersion effects.

Acknowledgment

The authors are indebted to Didier Sébilleau (IPR Rennes, France) for suggesting this research topic. A.L. acknowledges support from the Swedish Research Council (Grant n° 2014–6463) and Marie Sklodowska Curie Actions (Cofund. Project INCA 600398). We thank HZB for the allocation of synchrotron radiation beamtime.

Appendix A

Photoelectron inelastic scattering in anisotropic crystals

In this Appendix, we estimate the sensitivity of measured HAXPES-PEELS spectra to the material anisotropy. After elimination of multiple inelastic scattering events, one obtains the q-averaged bulk ELF, $< \mathrm{Im}(-1/\varepsilon(\omega, q)) >_q$, this weighted average being obtained over the physically allowed space of q wave vectors. In photoelectron energy loss experiments, due to the longitudinal type of

excitation, the direction of the wave vector q corresponds to that of the electric field E in the optical experiments. Photoelectron scattering in anisotropic solids is determined by the direction of the momentum q transferred to plasmon excitations with respect to the principal axes of the crystal; it depends on scattering angle, energy loss value and initial direction of the photoelectron. Hence, due to the biaxial anisotropy of the dielectric function of BPh, the measured ELF will depend on the geometry of the HAXPES-PEELS experiment.

Several factors are considered including X-ray incidence, X-ray polarization, photoemission angle, photoelectron kinetic energy (Section a) along with the critical scattering angle in the plasmon excitation (Section b). Photoelectron spectroscopy at normal emission angle generally coincides with the out-of-plane direction (z = ***c*** axis in graphite, z = ***b*** axis in the orthorhombic BPh crystal). In a single inelastic scattering event, energy and momentum conservation rules define the direction of the q wave vector transferred to the plasmon, with respect to the principal axes of the crystal (Section c). In anisotropic solids, the measured "effective" ELF thus depends on the energy loss value and it is averaged over scattering angle distribution and initial photoelectron direction. Depending on material composition and photoelectron kinetic energy, elastic scattering may have additional randomizing effect on the q wave vector orientation (Section d). The relative importance of each mechanism is illustrated by considering HAXPES data for P 1s photoelectrons in BPh.

a) Differential photoelectric cross section

For a linearly polarized X-ray beam, the angular distribution of photoelectrons is given by the differential photoelectric cross-section **[53]**:

$$\frac{d\sigma_{nl}}{d\Omega} = \left(\frac{\sigma_{nl}}{4\pi}\right)\left[1 + \frac{\beta_{nl}}{2}(3cos^2\psi - 1)\right]$$

where ψ is the angle between X-ray polarization and electron emission directions. In this study, for grazing X-ray incidence and polarization normal to the surface, emission of primary photoelectrons is maximized at normal emission ($\psi = 0$). For the P 1s core level (subshell anisotropy parameter $\beta_{nl} = 2$), the square bracket $[1 + \beta_{nl}] = 3$ at normal emission and drops by 10% at ± 18°. Since, for each loss energy value, the measured electron flux is averaged over the acceptance angle ($\pm \vartheta_{\mathrm{ACC}}$), this slight anisotropy in photoelectric cross section is neglected.

b) Critical scattering angle in BPh

Inelastic scattering angles are limited to a narrow angular range ($\vartheta < \vartheta_{\mathrm{C}}$) due to plasmon decay into electron-hole pairs; this critical angle is important to obtain the kinematic factor or Bethe-Born factor for normalization of the loss energy dependence **[57-59]**. Considering BPh as a nearly free

electron metal with five valence electrons and atom density N_{AT} = 5.23×10^{28} m^{-3}, the resulting Fermi energy E_F = 14.9 eV is in reasonable agreement with recent calculations **[25]**. The free electron plasmon energy is expected at $E_{P\,FE}$ = 19.0 eV, hence q_C = 12.7 nm^{-1}. For P 1s core level photoelectrons excited by hard X-rays at 6015 eV (E_0= 3870 eV), the critical scattering angle is $\vartheta_C = (q_C/k_0) =$ 40 mrad (2.3°).

c) Transferred wave vector orientation

In order to estimate the sensitivity of HAXPES-PEELS to crystal anisotropy, we consider here a single inelastic event (i.e. neglecting elastic scattering and multiple inelastic scattering) defined by the initial (k_0, E_0) and final (k_1, $E_0 - T$) values of the photoelectron wave vector and kinetic energy, corresponding to a scattering angle ϑ = (k_0, k_1). Energy and momentum conservation rules provide the momentum q transferred to a bulk plasmon:

$$q^2 = 2\,k_0{}^2\left[1 - \vartheta_T - (1 - 2\,\vartheta_T)^{1/2} cos(\vartheta)\right]$$

and its components oriented parallel and perpendicular to the incident trajectory (k_0), respectively:

$$(q_{\parallel}) = k_0 - k_1 \cos\vartheta \approx \vartheta_T\,k_0 \quad \text{and} \quad (q_{\perp}) = k_1\,sin\,\vartheta \approx \vartheta\,k_0$$

where $\vartheta_T = (T/2E_0)$. As the electron scattering angle increases, the direction of momentum transfer q changes from being parallel to perpendicular to the initial electron trajectory, with a cross-over at $\vartheta = \vartheta_T$. In HAXPES experiments, the large photoelectron kinetic energy leads to small values of the parallel wave vector component (q), hence significant scattering probability will be limited to small q values with a probability given by the kinematic factor $\vartheta/(\vartheta_T{}^2 + \vartheta^2)$.

In BPh, the initial kinetic energy, E_0 = 3870 eV, and wave vector, k_0 = 218.3 nm^{-1}, are given by the binding energy of P 1s photoelectrons. For plasmon excitation energy $T = E_P$ = 20 eV, ϑ_T = 2.6 mrad (0.15°) and the physically allowed wave vector values are between q^- = 0.84 nm^{-1} (ϑ = 0) and q_C = 12.7 nm^{-1} (ϑ_C = 40 mrad).

The q wave vector components parallel and perpendicular to the incident photoelectron wave vector (k_0), provide its projections onto the principal axes of the anisotropic crystal. For an angle (α) between the out-of-plane z axis and the incident electron k_0, the components of the transferred wave vector, q, along the directions parallel and perpendicular to the z axis being (q_z) = $q_{\parallel} cos(\alpha) + q_{\perp} sin(\alpha)$ and (q_{xy}) = $q_{\parallel} sin(\alpha) - q_{\perp} cos(\alpha)$, its orientation with respect to the out-of-plane z axis, given by the angle β = (z, q), depends on the initial kinetic energy (E_0) and the loss energy (T) through $\vartheta_T = (T/2E_0)$:

$$cos(\beta) = \left|\frac{q_z}{q}\right| = \frac{\vartheta_T cos(\alpha) + \vartheta sin(\alpha)}{\left[\vartheta_T{}^2 + \vartheta^2\right]^{1/2}}$$

As shown in **Fig. A1**, in single inelastic scattering, the in-plane orientation ($cos\beta \approx 0$) is expected at very small loss energy or large scattering angle. As a consequence, in HAXPES, high kinetic energy values, E_0, favor in-plane orientations of the momentum transferred to plasmon excitations. However, a weak dependence of cos β on the initial orientation of the initial photoelectron direction (angle α between k_0 and z-axis up to 40°) is found, as illustrated for ϑ = 8 mrad (set of red curves). Since the scattering angle probability is given by the kinematic factor $\vartheta/\left(\vartheta_T{}^2 + \vartheta^2\right)$ which is maximum near ϑ_T, a narrow range of scattering angles (shown as bold vertical lines in **Fig. A1**) dominates the scattered intensity, e.g. 2 mrad < ϑ < 4 mrad at 20 eV, corresponding to β values in the range 30°-60°. Hence, in HAXPES experimental conditions, plasmon excitation provides an efficient averaging of the anisotropic dielectric properties of BPh.

d) Influence of elastic scattering

The measured XPS spectrum contains photoelectrons which have suffered elastic scattering events before or after plasmon excitation. In contrast with inelastic electron scattering, elastic scattering is a broad-angle mechanism which contributes to some additional randomization. The differential elastic cross-section for P 1s photoelectrons (E_0 = 3870 eV) at small elastic scattering angles [**76**] is approximated by a Gaussian with half width ϑ_E = 3° = 52 mrad; the latter is significantly wider than the angular distribution allowed for plasmon excitation ($\theta < \vartheta_C$ = 40 mrad).

In XPS experiments, elastic deflections increase the electron path length through the solid before escaping the solid surface [**77**]. For high energy photoelectrons, this effect can be safely neglected because the differential cross section is strongly peaked in the forward direction; in addition, for HAXPES of BPh, the total elastic cross section, $\sigma_E(P) = 1.86\, a_0^2$ at E_0= 3870 eV, is rather small [**76**]. This situation is typical of atoms with low Z value.

Elastic scattering may have important consequences in anisotropic crystals because it contributes to broaden the initial wave vector distribution of photoelectrons measured along a given direction **[59]**. The mean free path between elastic scattering events, $\left(\sigma_E\, N_{AT}\right)^{-1}$ = 4.12 nm, obtained from the atom density N_{AT} = 5.23×10^{28} m^{-3}, is smaller than the photoelectron IMFP, $\lambda(E_0$ = 3870 eV) ≈ 7.7 nm in BPh (**[52]**). Hence, statistically, most photoelectrons which have excited one plasmon have also experienced at least one elastic scattering before or after the inelastic scattering event. This effect increases after multiple plasmon excitations, for photoelectrons originated from deeper

positions in the crystal. However, in this work, since the acceptance angle of the analyser, $\vartheta_{\mathrm{ACC}} = \pm 16°$, is much wider than ϑ_{E}, the measured photoelectron flux includes multiple elastic scattering events and fully incorporates their randomizing effect.

References

[1] A. Morita, Semiconducting Black Phosphorus, Appl. Phys. A 39 (1986) 227-242. DOI: 10.1007/BF00617267

[2] R. Hultgren, N.S. Gingrich, B.E. Warren, The Atomic Distribution in Red and Black Phosphorus and the Crystal Structure of Black Phosphorus, J. Chem. Phys. 3 (1935) 351-355. DOI: 10.1063/1.1749671

[3] A. Brown, S. Rundqvist, Refinement of the crystal structure of black phosphorus, Acta Cryst. 19 (1965) 684-685. DOI: 10.1107/S0365110X65004140

[4] L.H de Lima, L. Barreto, R. Landers, A. de Siervo, Surface Structure of Black Phosphorus Using Photoelectron Diffraction, Phys. Rev. B 93 (2017) 035448. DOI: 10.1103/PhysRevB.93.035448

[5] R. Gusmão, Z. Sofer, M. Pumera, Black Phosphorus Rediscovered: From Bulk Material to Monolayers, Angew. Chem. Int. Ed. 56 (2017) 8052-8072. DOI: 10.1002/anie.201610512

[6] F. Wang, Z. Wang, L. Yin, R. Cheng *et al.*, 2D library beyond graphene and transition metal dichalcogenides: a focus on photodetection. Chem. Soc. Rev. 47 (2018) 6296-6341. DOI: 10.1039/c8cs00255j

[7] F. Xia, H. Wang, Y. Jia, Rediscovering black phosphorus as an anisotropic layered material for optoelectronics and electronics, Nat. Commun. 5 (2014) 4458. DOI:10.1038/ncomms5458

[8] X. Ling, H. Wang, S. Huang, F. Xia, M.S. Dresselhaus, The Renaissance of Black Phosphorus, Proc. Natl. Acad. Sci. 112 (2015) 201416581. DOI: 10.1073/pnas.1416581112

[9] Y. Zhao, Y. Chen, Y.H. Zhang, S.F. Liu, Recent advance in black phosphorus: Properties and applications, Mater. Chem. Phys. 189 (2017) 215-229. DOI: 10.1016/j.matchemphys.2016.12.014

[10] R. Keyes, The electrical properties of black phosphorus, Phys. Rev. 92 (1953) 580-584. DOI: 10.1103/PhysRev.92.580

[11] D. Warschauer, Electrical and optical properties of crystalline black phosphorus, J. Appl. Phys. 34 (1963) 1853-1860. DOI: 10.1063/1.1729699

[12] Y. Maruyama, S. Suzuki, K. Kobayashi, S. Tanuma, Synthesis and some properties of black phosphorus single crystals, Physica B+C 105 (1981) 99-102. DOI: 10.1016/0378-4363(81)90223-0

[13] Y. Akahama, S. Endo, S.I. Narita, Electrical properties of black phosphorus single crystals, J. Phys. Soc. Jpn. 52 (1983) 2148-2155. DOI: 10.1143/JPSJ.52.2148

[14] H. Asahina, A. Morita, Band structure and optical properties of black phosphorus, J. Phys. C 17 (1984) 1839-1852. DOI: 10.1088/0022-3719/17/11/006

[15] S. Narita, S. Terada, S. Mori, K. Muro, Y. Akahama, S. Endo, Far-Infrared Cyclotron Resonance Absorptions in Black Phosphorus Single Crystals, J. Phys. Soc. Jpn. 52 (1983) 3544-3553. DOI: 10.1143/JPSJ.52.3544

[16] L. Li, Y. Yu, G.J. Ye *et al.*, Black phosphorus field-effect transistors, Nature Nanotechnol. 9 (2014) 372–377. DOI: 10.1038/nnano.2014.35

[17] Y. Yi, X.F. Yu, W. Zhou, J. Wang, P.K. Chu, Two-dimensional black phosphorus: Synthesis, modification, properties, and applications. Mater. Sci. Eng. R 120 (2017) 1-33. DOI: 10.1016/j.mser.2017.08.001

[18] H. Yuan, X. Liu, F. Afshinmanesh, W. Lei *et al.*, Polarization-sensitive broadband photodetector using a black phosphorus vertical p–n junction, Nature Nanotechnol. 10 (2015) 707–713. DOI: 10.1038/nnano.2015.112

[19] D. Correas-Serrano, A. Alù, J.S. Gomez-Diaz, Plasmon canalization and tunneling over anisotropic metasurfaces, Phys. Rev. B 96 (2017) 075436. DOI: 10.1103/PhysRevB.96.075436

[20] P.K. Venuthurumilli, P.D. Ye, X. Xu, Plasmonic Resonance Enhanced Polarization-Sensitive Photodetection by Black Phosphorus in Near Infrared, ACS Nano 12 (2018) 4861–4867. DOI: 10.1021/acsnano.8b01660

[21] S. Lin, Y. Li, J. Qian, S.P. Lau, Emerging opportunities for black phosphorus in energy applications, Materials Today Energy 12 (2019) 1-25. DOI: 10.1016/j.mtener.2018.12.004

[22] Y. Takao, H.Asahina, A.Morita, Electronic Structure of Black Phosphorus in Tight Binding Approach, J. Phys. Soc. Jpn. 50 (1981) 3362-3369. DOI: 10.1143/JPSJ.50.3362

[23] A.N. Rudenko, S. Yuan, M.I. Katsnelson, Toward a realistic description of multilayer black phosphorus: From GW approximation to large-scale tight-binding simulations, Phys. Rev. B 92 (2015) 085419. DOI: 10.1103/PhysRevB.92.085419

[24] H. Asahina, K. Shindo, A. Morita, Electronic structure of black phosphorus in self-consistent pseudopotential approach, J. Phys. Soc. Jpn. 51 (1982) 1193. DOI: 10.1143/JPSJ.51.1193

[25] L. Craco, T.A. da Silva Pereira, S. Leoni, Electronic structure and thermoelectric transport of black phosphorus, Phys. Rev. B 96 (2017) 075118. DOI: 10.1103/PhysRevB.96.075118

[26] B. Nolang, O. Eriksson, B. Johansson, The cohesive energy and band structure of black phosphorus, J. Phys. Chem. Solids 51 (1990) 1025-1032. DOI: 10.1016/0022-3697(90)90061-J

[27] Y. Du, C. Ouyang, S. Shi, M. Lei, Ab initio studies on atomic and electronic structures of black phosphorus, J. Appl. Phys. 107 (2010) 093718. DOI: 10.1063/1.3386509

[28] R. Schuster, J. Trinckauf, C. Habenicht, M. Knupfer, B. Büchner, Anisotropic Particle-Hole Excitations in Black Phosphorus, Phys. Rev. Lett. 115 (2015) 026404. DOI: 10.1103/PhysRevLett.115.026404

[29] X.P. Kong, X. Shen, J. Jang, X. Gao, Electron Pair Repulsion Responsible for the Peculiar Edge Effects and Surface Chemistry of Black Phosphorus. J. Phys. Chem. Lett. 9 (2018) 947-953. DOI: 10.1021/acs.jpclett.8b00128

[30] E. Golias, M. Krivenkov, J. Sánchez-Barriga, Disentangling bulk from surface contributions in the electronic structure of black phosphorus, Phys. Rev. B 93 (2016) 075207. DOI: 10.1103/PhysRevB.93.075207

[31] Y. Harada, K. Murano, I. Shirotani, T. Takahashi, Y. Maruyama, Electronic structure of black phosphorus studied by X-ray photoelectron spectroscopy, Solid State Commun. 44 (1982) 877-879. DOI: 10.1016/0038-1098(82)90295-2

[32] M. Taniguchi, S. Suga, M. Seki, H. Sakamoto, H. Kanzaki, Y. Akahama, S. Terada, S. Endo, S. Narita, Valence band and core-level photoemission spectra of black phosphorus, Solid State Commun. 45 (1983) 59-61. DOI: 10.1016/0038-1098(83)90340-X

[33] N.B. Goodman, L. Ley, D.W. Bullett, Valence-band structures of phosphorus allotropes, Phys. Rev. B 27 (1983) 7440-7450. DOI: 10.1103/PhysRevB.27.7440

[34] T. Takahashi, H. Tokailin, S. Suzuki, T. Sagawa, I. Shirotani, Electronic band structure of black phosphorus studied by angle-resolved ultraviolet photoelectron spectroscopy, J. Phys. C 18 (1985) 825-836. DOI: 10.1088/0022-3719/18/4/013

[35] C.Q. Han, M.Y. Yao, X.X. Bai, L. Miao, F. Zhu, D.D. Guan, S. Wang, C.L. Gao, C. Liu, D. Qian, Y. Liu, J.F. Jia, Electronic structure of black phosphorus studied by angle-resolved photoemission spectroscopy, Phys. Rev. B 90 (2014) 085101. DOI: 10.1103/PhysRevB.90.085101

[36] R.J. Wu, M. Topsakal, T. Low, M.C. Robbins, N. Haratipour, J.S. Jeong, R.M. Wentzcovitch, S.J. Koester, K.A. Mkhoyan, Atomic and electronic structure of exfoliated black phosphorus, J. Vac. Sci. Technol. A 33 (2015) 060604. DOI: 10.1116/1.4926753

[37] W. Luo, D.Y. Zemlyanov, C.A. Milligan, Y. Du, L. Yang, Y. Wu, P.D. Ye, Surface chemistry of black phosphorus under a controlled oxidative environment, Nanotechnol. 27 (2016) 434002. DOI: 10.1088/0957-4484/27/43/434002

[38] T. Ahmed, S. Balendhran, M.N. Karim, E.L.H. Mayes, M.R. Field, R. Ramanathan, M. Singh, V. Bansal, S. Sriram, M. Bhaskaran, S. Walia, Degradation of black phosphorus is contingent on UV–blue light exposure, npj 2D Materials and Applications 1 (2017) 434002. DOI: 10.1038/s41699-017-0023-5

[39] A. Favron, E. Gaufrès, F. Fossard, A.L. Phaneuf-L'Heureux, N.Y.W. Tang, P.L. Lévesque, *et al.* Photooxidation and quantum confinement effects in exfoliated black phosphorus. Nature Materials 14 (2015) 826-832. DOI: 10.1038/nmat4299

[40] J. Cazaux, Dielectric constant and electron energy losses in solids having two separated groups of filled bands (energy range 3–30 eV), Opt. Commun. 3 (1971) 221-224. DOI: 10.1016/0030-4018(71)90007-1

[41] J.A. Leiro, M.H. Heinonen, T. Laiho, I.G. Batirev, Core-level XPS spectra of fullerene, highly oriented pyrolitic graphite, and glassy carbon, J. Electron Spectrosc. Relat. Phenom. 128 (2003) 205-213. DOI: 10.1016/S0368-2048(02)00284-0

[42] A. Kumar, P.K. Ahluwalia, Tunable dieclectric response of transition metal dichalcogenides MX_2 (M=Mo, W; X=S, Se, Te): Effect of quantum confinement, Physica B 407 (2012) 4627-4634. DOI: 10.1016/j.physb.2012.08.034

[43] M.G. Bell, W.Y. Liang, Electron energy loss studies in solids; The transition metal dichalcogenides, Adv. Phys. 25 (1976) 53-86. DOI: 10.1080/00018737600101362

[44] A. Politano, G. Chiarello, C. Spinella, Plasmon spectroscopy of graphene and other two-dimensional materials with transmission electron microscopy, Mater. Sci. Semicond. Process. 65 (2017) 88-99. DOI: 10.1016/j.mssp.2016.05.002

[45] F. Fossard, L. Sponza, L. Schué, C. Attaccalite, F. Ducastelle, J. Barjon A. Loiseau, Angle-resolved electron energy loss spectroscopy in hexagonal boron nitride, Phys. Rev. B 96 (2017) 115304. DOI: 10.1103/PhysRevB.96.115304

[46] N. Pauly, S. Tougaard, Surface excitation parameter for 12 semiconductors and determination of a general predictive formula, Surf. Interf. Anal. 41 (2009) 735-740. DOI: 10.1002/sia.3081

[47] V.M. Santana, D. David, J.S. de Almeida, C. Godet, Photoelectron energy-loss in Al(002) revisited : retrieval of the single plasmon loss energy distribution by a Fourier transform method, Braz. J. Phys. 48 (2018) 215-226. DOI: 10.1007/s13538-018-0566-8

[48] G.K. Wertheim, P.H. Citrin, Fermi Surface Excitations in X-Ray Photoemission Line Shapes from Metals, in: M. Cardona, L. Ley (eds), Photoemission in Solids I, Springer, Berlin / Heidelberg, 1978, pp. 197-236.

[49] S. Doniach, M. Sunjic, Many-electron singularity in x-ray photoemission and-ray line spectra from metals, J. Phys. C: Solid State Phys. 3 (1970) 285-291. DOI: 10.1088/0022-3719/3/2/010

[50] F. Schaefers, M. Mertin, M. Gorgoi, KMC-1: A High Resolution and High Flux Soft x-Ray Beamline at BESSY. Rev. Sci. Instrum. 78 (2007) 123102. DOI: 10.1063/1.2808334

[51] M. Gorgoi, S. Svensson, F. Schaefers, G. Ohrwall, M. Mertin, P. Bressler, *et al.* (2009). The high kinetic energy photoelectron spectroscopy facility at BESSY progress and first results. Nucl. Instrum. Methods Phys. Res. A 601 (2009) 48-53. DOI: 10.1016/j.nima.2008.12.244

[52] S. Tanuma, C.J. Powell, D.R. Penn, Calculations of electron inelastic mean free paths. VIII. Data for 15 elemental solids over the 50-2000 eV range, Surf. Interf. Anal. 36 (2004) 1-14. DOI: 10.1002/sia.1997

[53] J.W. Cooper, Photoelectron-angular-distribution parameters for rare-gas subshells, Phys. Rev. A 47 (1993) 1841-1851. DOI: 10.1103/PhysRevA.47.1841

[54] www.hqgraphene.com

[55] R. Franke, T. Chasse, P. Steubel, A. Meisel, Auger parameters and relaxation energies of phosphorus in solid compounds, J. Electron Spectrosc. Relat. Phenom. 56 (1991) 381-388. DOI: 10.1016/0368-2048(91)85035-R

[56] H. Raether, *Excitation of Plasmons and Interband Transitions by Electrons*, Springer Tracts in Modern Physics, Vol. 88, Springer-Verlag, Berlin, 1997.

[57] D. David, C. Godet, Derivation of dielectric function and inelastic mean free path from photoelectron energy-loss spectra of amorphous carbon surfaces, Appl. Surf. Sci. 387 (2016) 1125-1139. DOI: 10.1016/j.apsusc.2016.06.044

[58] L. Calliari, S. Fanchenko, Reflection electron energy loss spectroscopy: role of the Bethe–Born factor, Surf. Interf. Anal. 44 (2012) 1104-1109. DOI: 10.1002/sia.4827

[59] R.F. Egerton, Electron Energy-Loss Spectroscopy in the Electron Microscope, Plenum Press, New York, 1986, p. 190.

[60] W.J. Pardee, G.D. Mahan, D.E. Eastman, R.A. Pollak, L. Ley, F.R. McFeely, S.P. Kowalczyk, D.A. Shirley, Analysis of surface- and bulk-plasmon contributions to x-ray photoemission spectra, Phys. Rev. B 11 (1975) 3614-3616. DOI: 10.1103/PhysRevB.11.3614

[61] C. Godet, V.M. Santana, D. David, Depth distribution of noble gas atoms implanted in Al matrix: a photoelectron energy loss spectroscopy study, Thin Solid Films 659 (2018) 70-80. DOI: 10.1016/j.tsf.2018.05.038

[62] X. Gonze, J.M. Beuken, R. Caracas, F. Detraux, M. Fuchs, G.M. Rignanese, M. Torrent, First-principles computation of material properties: The ABINIT software project. Comput. Mater. Sci. 25 (2002) 478-492. DOI: 10.1016/S0927-0256(02)00325-7

[63] A.D. Boese, N.L. Doltsinis, N.C. Handy, M. Sprik, New generalized gradient approximations, J. Chem. Phys. 112 (2000) 1670-1678. DOI: 10.1063/1.480732

[64] J.P. Perdew, S. Burke, M. Ernzerhof, Generalized gradient approximation made simple. Phys. Rev. Lett. 77 (1996) 3865-3868. DOI: 10.1103/PhysRevLett.77.3865

[65] www.aflowlib.org/CrystalDatabase/A_oC8_64_f.P.html

[66] H.J. Monkhorst, J.D. Pack, Special points for Brillouin-zone integrations. Phys. Rev. B 13 (1976) 5188-5192. DOI: 10.1103/PhysRevB.13.5188

[67] J. Daniels, C.v. Festenberg, H. Raether, K. Zeppenfeld, Springer Tracts in Modern Physics, Vol. 54, Springer-Verlag, Berlin, 1970, p. 78-135.

[68] C. Kaneta, H. Katayama-Yoshida, A. Morita, Lattice dynamics of black phosphorus, Solid State Commun. 44 (1982) 613-617. DOI: 10.1143/JPSJ.55.1213

[69] E. Gaufrès, A. Favron, F. Fossard, P. Lévesque, *et al.*. Spectroscopy on Black Phosphorus exfoliated down to the monolayer. 16th European Microscopy Congress, 2016, Lyon, France. Wiley-VCH, Material Science 2.1, p. 478, 2016, EMC2016. DOI: 10.1002/9783527808465.EMC2016.6100

[70] G. Nicotra, E. Van Veen, I. Deretzis, L. Wang *et al.*, Anisotropic ultraviolet-plasmon dispersion in black phosphorus, Nanoscale 10 (2018) 21918-21927. DOI: 10.1039/c8nr05502e

[71] J.J. Quinn, Bulk and surface plasmons in solids, Nucl. Instrum. Methods Phys. Res. B 96 (1995) 460-464. DOI : 10.1016/0168-583X(95)00246-4

[72] H.K. Sy, T.C. Chua, Plasmons in a Superlattice with a Doped Surface Layer, Phys. Stat. Sol. (b) 176 (1993) 131-141. DOI: 10.1002/pssb.2221760113

[73] P.J. Feibelman, Surface electromagnetic fields, Prog. Surf. Sci. 12 (1982) 287-408. DOI: 10.1016/0079-6816(82)90001-6

[74] P. Cudazzo, K.O. Ruotsalainen, C.J. Sahle, A. Al-Zein, H. Berger, E. Navarro-Moratalla, S. Huotari, M. Gatti, A. Rubio, High-energy collective electronic excitations in layered transition-metal dichalcogenides, Phys. Rev. B 90 (2014) 125125. DOI: 10.1103/PhysRevB.90.125125

[75] A.G. Marinopoulos, L. Reining, V. Olevano, A. Rubio, T. Pichler, X. Liu, M. Knupfer, J. Fink, Anisotropy and Interplane Interactions in the Dielectric Response of Graphite, Phys. Rev. Lett. 89 (2002) 076402. DOI: 10.1103/PhysRevLett.89.076402

[76] Elastic scattering cross section: see https://srdata.nist.gov

[77] A. Jablonski, C. Powell, Practical expressions for the mean escape depth, the information depth, and the effective attenuation length in Auger-electron spectroscopy and x-ray photoelectron spectroscopy, J. Vac. Sci. Technol. A 27 (2009) 253-261. DOI: 10.1116/1.3071947

Fig. 1. Schematic illustration of the atomic structure and principal axes of the orthorhombic BPh crystal (in-plane armchair ***c*** = x, in-plane zig-zag ***a*** = y, out-of-plane ***b*** = z): (a) Side view (bc plane) showing three bilayers (or three phosphorene layers). The P atoms are shown in different gray scales for clarity. (b) Top view (ac plane) showing two bilayers and the in-plane unit cell. Adapted from de Lima *et al.* [**4**].

Fig. 2. HAXPES current (logarithmic scale) as a function of apparent binding energy (with respect to the Fermi level) for P 1s core level photoelectrons emitted at normal emission angle from a cleaved black phosphorus crystal. Inset: surface-sensitive spectrum obtained at lower X-ray energy (3100 eV) showing weak surface contamination, C 1s and O 1s (log scale).

Fig. 3. Normalized HAXPES-PEELS spectrum of P 1s photoelectrons in BPh, before and after removal of a symmetrical ZLP (blue line); the onset of energy losses is linearly extrapolated to $E_G \approx$ 0.3 eV. High energy collective excitations include a bulk plasmon peak BP1 at 20 eV. Low energy losses are attributed to inter band transitions (labelled according to the residual signal obtained in **Fig. 4b**).

Fig. 4. a) Raw HAXPES data (red) and single energy loss function (black) of BPh derived from the FT method. b) Analytic decomposition of the ELF into bulk and surface plasmon excitations. The residual signal (black curve) is attributed to inter band transitions up to 10 eV, and to some deviation of the BP1 line shape from a single Drude-Lorentz ELF at and below 20 eV.

Fig. 5. a) DFT calculated density of states; b) Comparison of inter band transition momentum (M_{11}, M_{10}, M_{01}, M_{00}) derived from the joint-density-of-states with the low energy ELF in PEELS.

Fig. 6. ABINIT calculation of the anisotropic electronic structure of BPh: Re(ε), Im(ε), Im(-1/ε). The ELF (BP1) is slightly broader for the zig-zag (y = **a**) direction. The star symbol emphasizes the location of the observed anomalous surface plasmon near 9 eV.

Fig. A1. Spectral dependence of the orientation of the wave vector, q = (k_0 - k_1), transferred to plasmon excitation (angle β with respect to the z normal-axis) as a function of scattering angle ($\vartheta < \vartheta_C$). The weak dependence of cos β on the initial orientation of the photoelectron direction (angle α between k_0 and z-axis) is shown for ϑ = 8 mrad. The scattering angle probability given by the kinematic factor $\vartheta/\left[\vartheta_T{}^2 + \vartheta^2\right]$ being maximum near ϑ_T, a narrow range of scattering angles (bold vertical lines) dominates the scattered intensity, e.g. 2 mrad < ϑ < 4 mrad at 20 eV. In HAXPES experimental conditions, plasmon excitation provides efficient averaging of the anisotropic dielectric properties

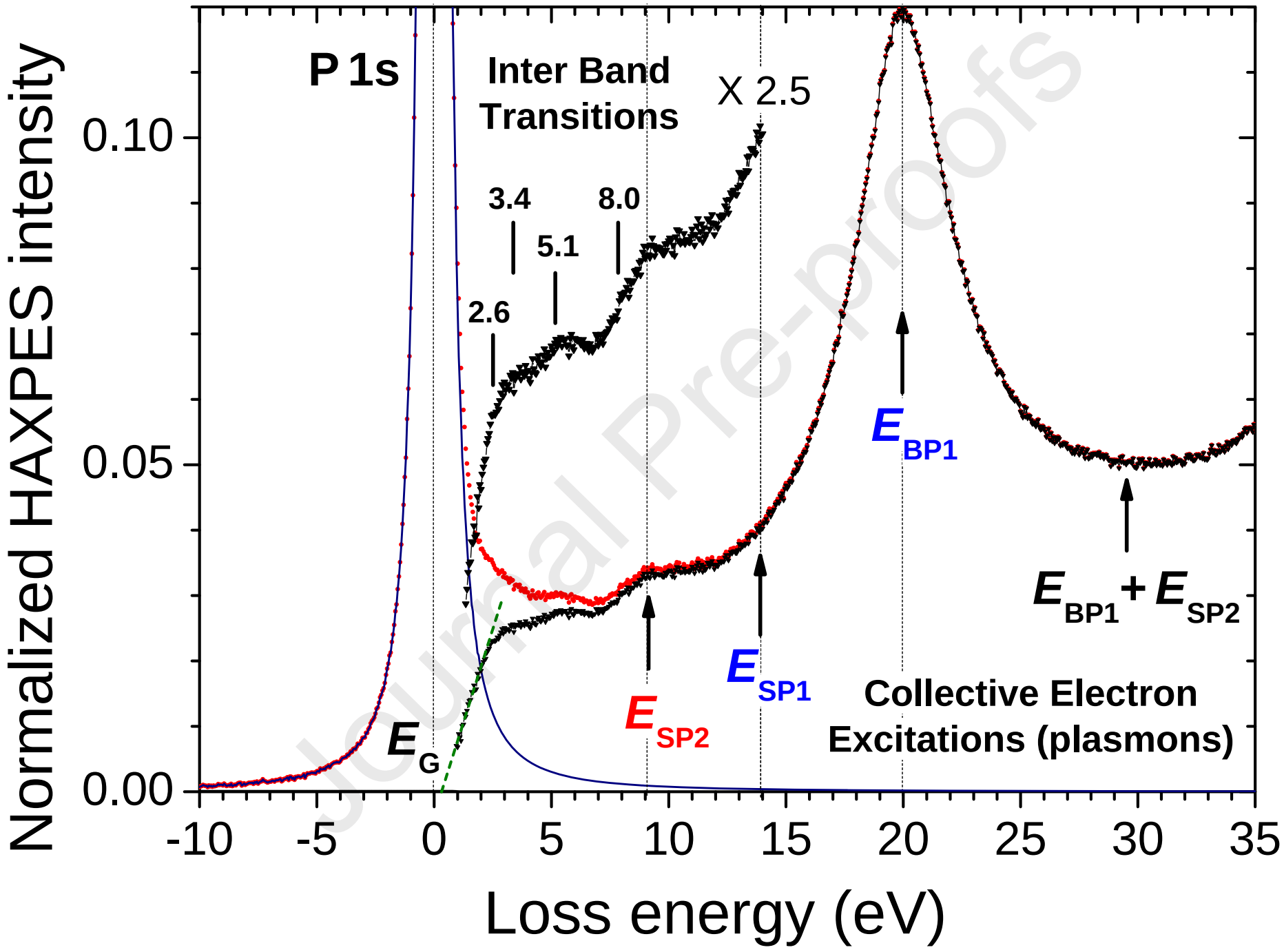

Highlights

- Energy loss distribution of P 1s photoelectrons in black phosphorus
- Energy loss function due to plasmon excitations and inter band transitions
- Anomalous surface plasmon resonance at 9 eV
- DFT calculated ELF tensor vs measured ELF

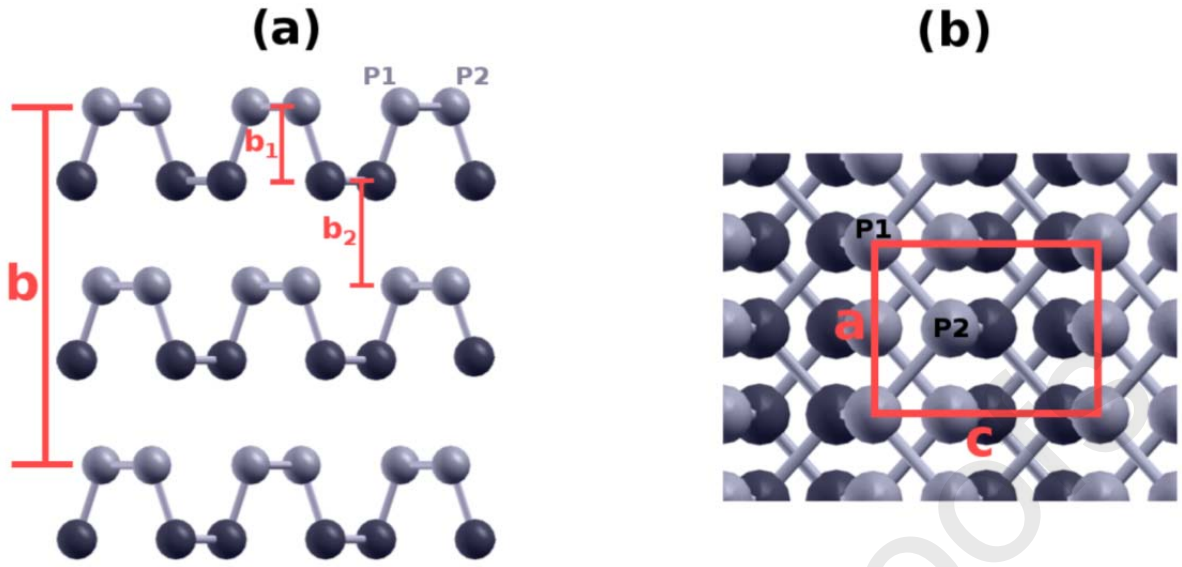

Figure 1: Schematic illustration of the atomic structure and principal axes of the orthorhombic BPh crystal (in-plane armchair ***c*** = x, in-plane zig-zag ***a*** = y, out-of-plane ***b*** = z): (a) Side view (bc plane) showing three bilayers (or three phosphorene layers). The P atoms are shown in different gray scales for clarity. (b) Top view (ac plane) showing two bilayers and the in-plane unit cell. Adapted from de Lima *et al.* [**4**].

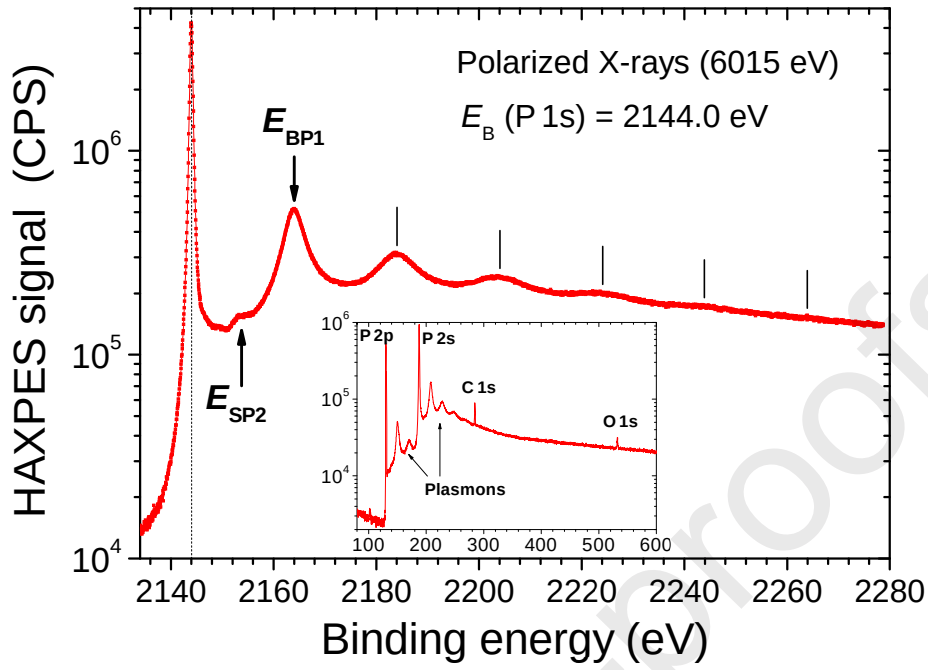

Figure 2: HAXPES current (logarithmic scale) as a function of apparent binding energy (with respect to the Fermi level) for P 1s core level photoelectrons emitted at normal emission angle from a cleaved black phosphorus crystal. Inset: surface-sensitive spectrum obtained at lower X-ray energy (3100 eV) showing P 2p and P 2s core levels (along with their respective plasmons) and weak surface contamination, C 1s and O 1s (log scale).

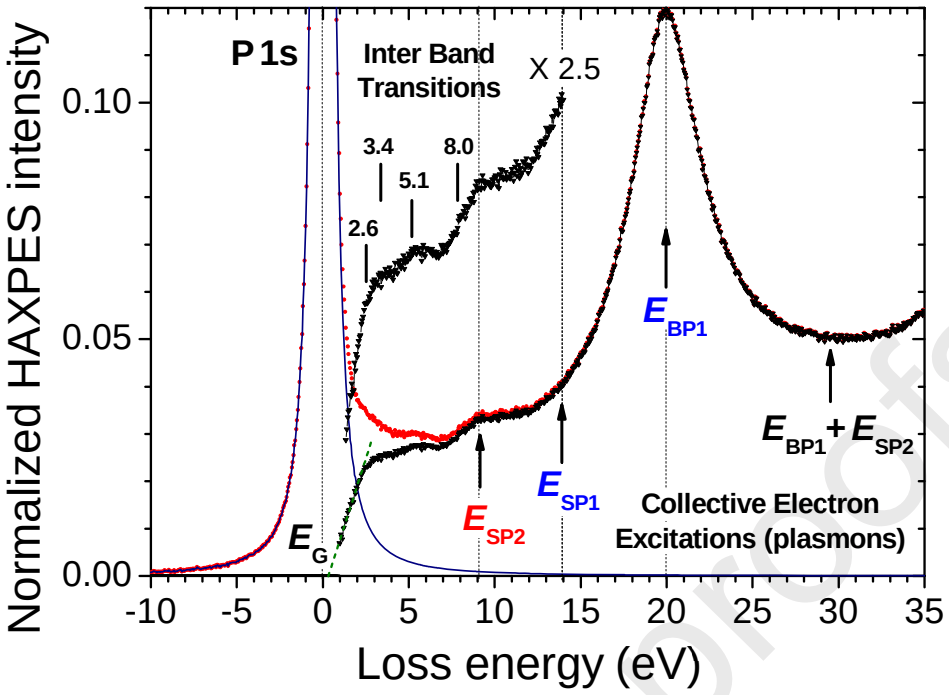

Figure 3: Normalized HAXPES-PEELS spectrum of P 1s photoelectrons in BPh, before and after removal of a symmetrical ZLP (blue line); the onset of energy losses is linearly extrapolated to $E_G \approx$ 0.3 eV. High energy collective excitations include a bulk plasmon peak BP1 at 20 eV along with surface excitations (see text). Low energy losses are attributed to inter band transitions (labelled according to the residual signal obtained in **Fig. 4b**).

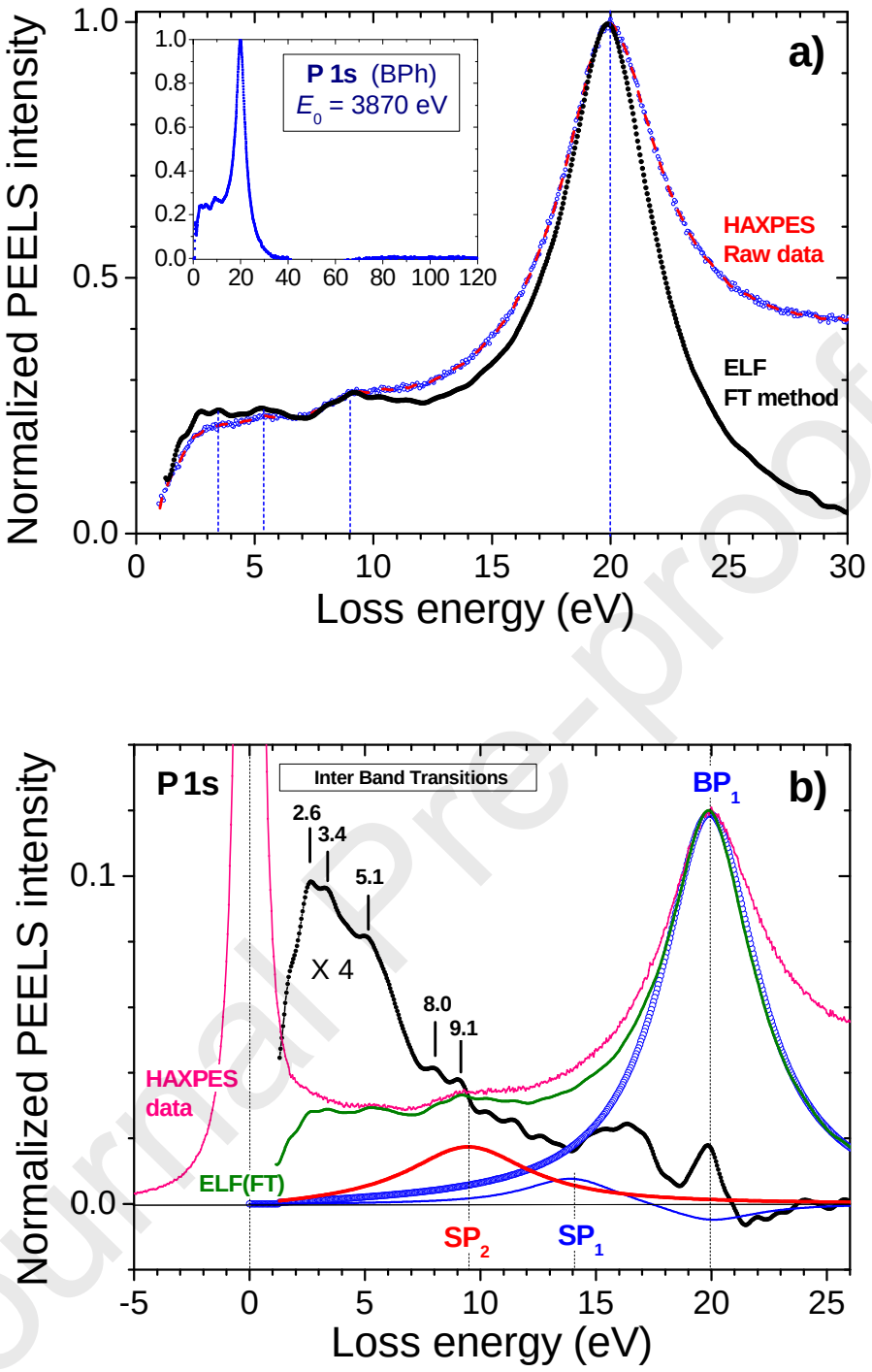

Figure 4: a) Raw HAXPES data (red) and single energy loss function (black) of BPh derived from the FT method. b) Analytic decomposition of the ELF into bulk and surface plasmon excitations. The residual signal (black curve) is attributed to inter band transitions up to 10 eV, and to some deviation of the BP1 line shape from a single Drude-Lorentz ELF at and below 20 eV.

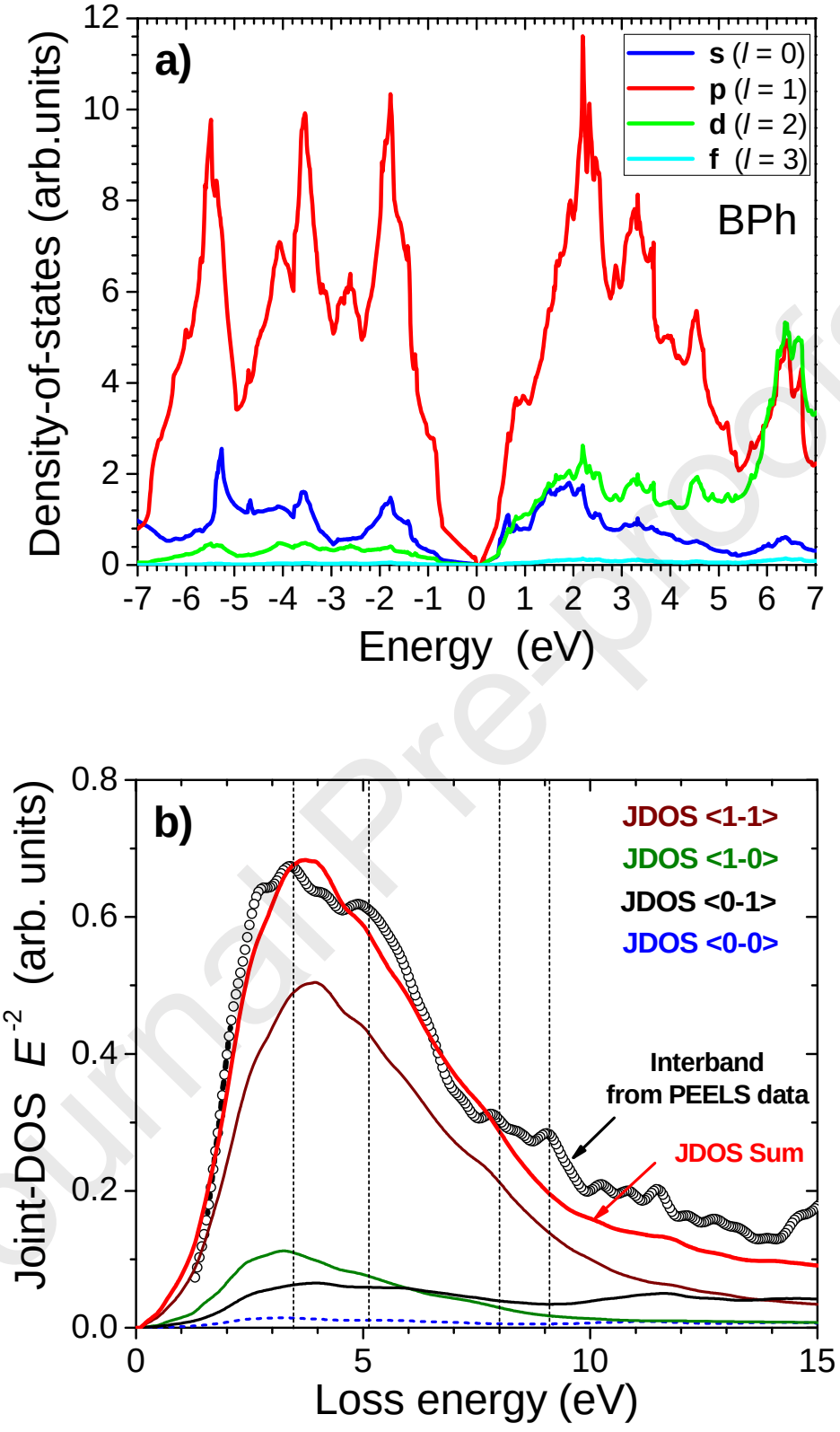

Figure 5: a) DFT calculated density of states; b) Comparison of inter band transition momentum (M_{11}, M_{10}, M_{01}, M_{00}) derived from the joint-density-of-states with the low energy ELF in PEELS.

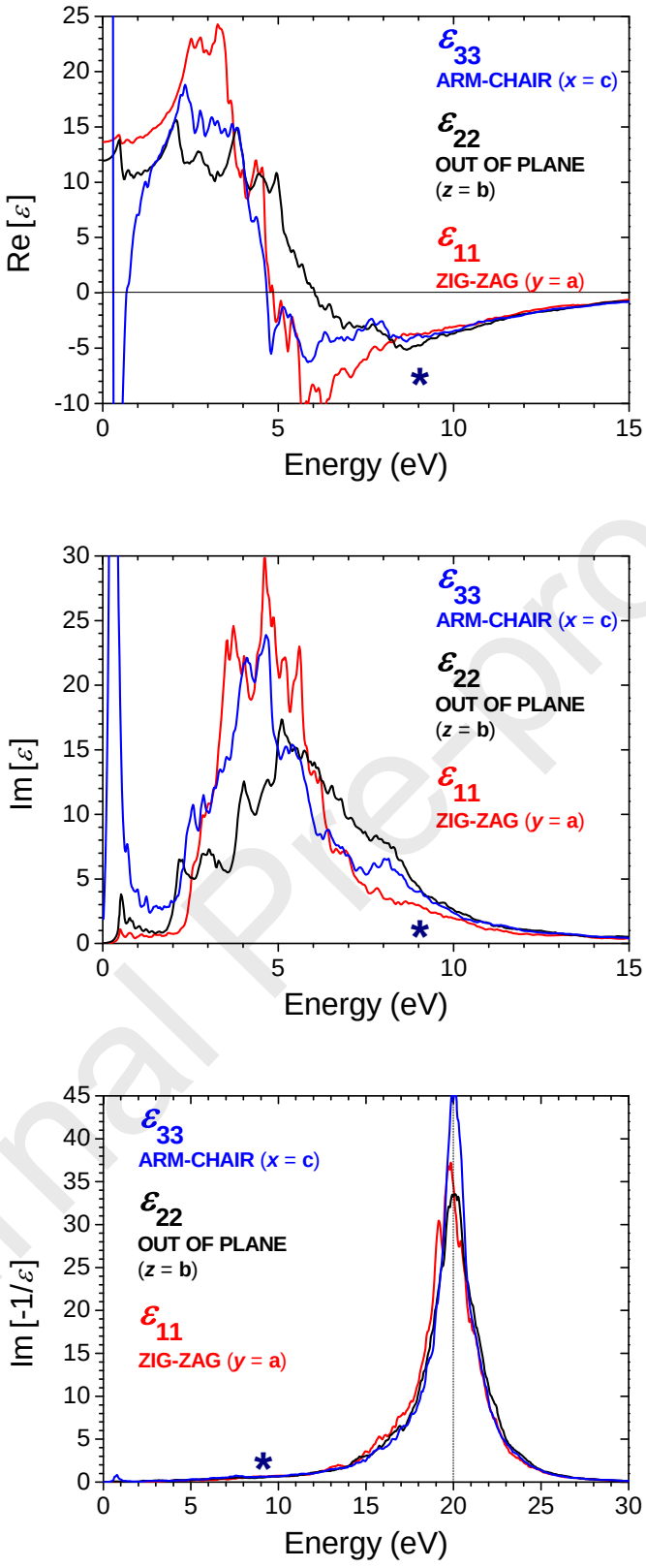

Figure 6: ABINIT calculation of the anisotropic electronic structure of BPh: Re(ε), Im(ε), Im(-1/ε). The ELF (BP1) is slightly broader for the zig-zag (y = **a**) direction. The star symbol indicates the location of the observed anomalous surface plasmon near 9 eV.

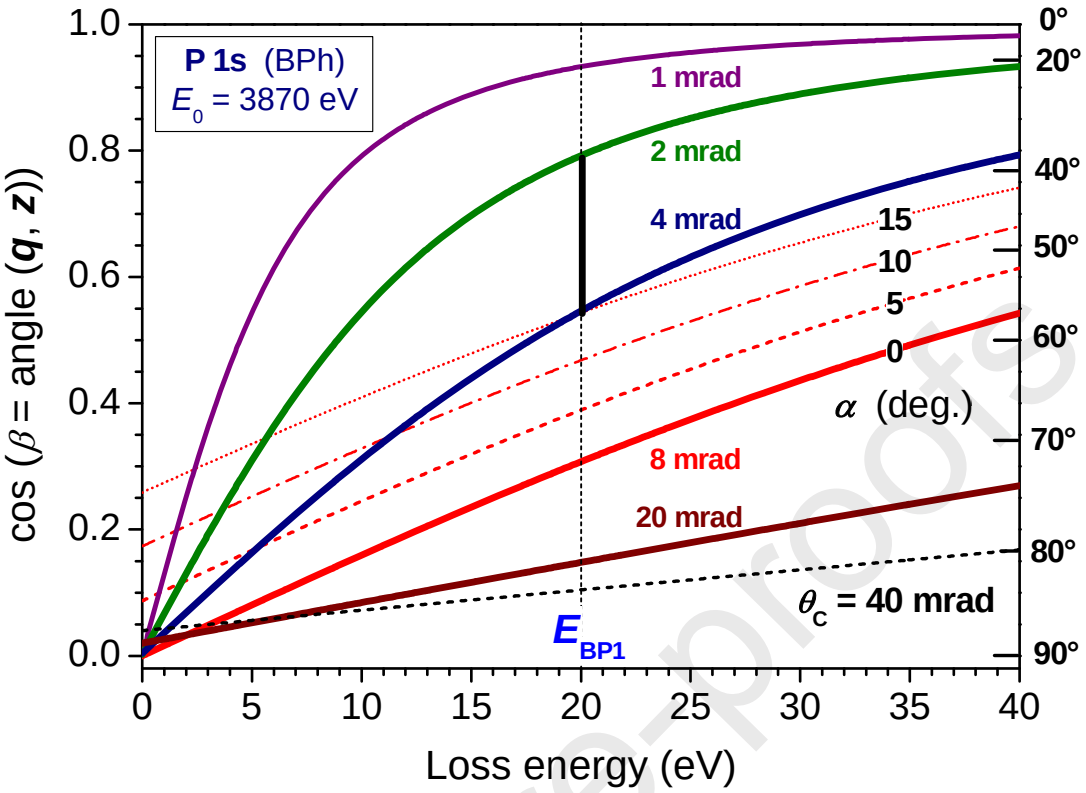

Figure A1 : Spectral dependence of the orientation of the wave vector, q = (k_0 - k_1), transferred to plasmon excitation (angle β with respect to the z normal-axis) as a function of scattering angle ($\vartheta < \vartheta_C$). The weak dependence of cos β on the initial orientation of the photoelectron direction (angle α between k_0 and z-axis) is shown for ϑ = 8 mrad. The scattering angle probability given by the kinematic factor $\vartheta/\left[\vartheta_T{}^2 + \vartheta^2\right]$ being maximum near ϑ_T, a narrow range of scattering angles (bold vertical lines) dominates the scattered intensity, e.g. 2 mrad < ϑ < 4 mrad at 20 eV. In HAXPES experimental conditions, plasmon excitation provides efficient averaging of the anisotropic dielectric properties.